Atmos. Chem. Phys., 23, 1863–1877, 2023
https://doi.org/10.5194/acp-23-1863-2023

Atmospheric Chemistry and Physics
Open Access
EGU

Particle number concentrations and size distributions in the stratosphere: implications of nucleation mechanisms and particle microphysics

Fangqun Yu[1], Gan Luo[1], Arshad Arjunan Nair[1], Sebastian Eastham[2,3], Christina J. Williamson[4,5,a,b], Agnieszka Kupc[5,6], and Charles A. Brock[5]

[1]Atmospheric Sciences Research Center, State University of New York at Albany, Albany, NY 12226, US
[2]Laboratory for Aviation and the Environment, Department of Aeronautics and Astronautics, Massachusetts Institute of Technology, Cambridge, MA 02139, USA
[3]Joint Program on the Science and Policy of Global Change, Massachusetts Institute of Technology, Cambridge, MA 02139, USA
[4]Cooperative Institute for Research in Environmental Sciences, University of Colorado, Boulder, CO 80309, USA
[5]Chemical Sciences Laboratory, National Oceanic and Atmospheric Administration, Boulder, CO 80305, USA
[6]Faculty of Physics, Aerosol Physics and Environmental Physics, University of Vienna, Vienna 1090, Austria
[a]now at: Climate Research Programme, Finnish Meteorological Institute, Helsinki 00101, Finland
[b]now at: Institute for Atmospheric and Earth System Research/Physics, Faculty of Science, University of Helsinki, Helsinki 00014, Finland

Correspondence: Fangqun Yu (fyu@albany.edu)

Received: 8 July 2022 – Discussion started: 27 July 2022
Revised: 14 December 2022 – Accepted: 15 December 2022 – Published: 2 February 2023

Abstract. While formation and growth of particles in the troposphere have been extensively studied in the past two decades, very limited efforts have been devoted to understanding these in the stratosphere. Here we use both Cosmics Leaving OUtdoor Droplets (CLOUD) laboratory measurements taken under very low temperatures (205–223 K) and Atmospheric Tomography Mission (ATom) in situ observations of particle number size distributions (PNSDs) down to 3 nm to constrain nucleation mechanisms and to evaluate model-simulated particle size distributions in the lowermost stratosphere (LMS). We show that the binary homogenous nucleation (BHN) scheme used in most of the existing stratospheric aerosol injection (a proposed method of solar radiation modification) modeling studies overpredicts the nucleation rates by 3–4 orders of magnitude (when compared to CLOUD data) and particle number concentrations in the background LMS by a factor $\sim$2–4 (when compared to ATom data). Based on a recently developed kinetic nucleation model, which gives rates of both ion-mediated nucleation (IMN) and BHN at low temperatures in good agreement with CLOUD measurements, both BHN and IMN occur in the stratosphere. However, IMN rates are generally more than 1 order of magnitude higher than BHN rates and thus dominate nucleation in the background stratosphere. In the Southern Hemisphere (SH) LMS with minimum influence of anthropogenic emissions, our analysis shows that ATom-measured PNSDs generally have four apparent modes. The model captures reasonably well the two modes (Aitken mode and the first accumulation mode) with the highest number concentrations and size-dependent standard deviations. However, the model misses an apparent second accumulation mode peaking around 300–400 nm, which is in the size range important for aerosol direct radiative forcing. The bimodal structure of accumulation mode particles has also been observed in the stratosphere well above tropopause and in the volcano-perturbed stratosphere. We suggest that this bimodal structure may be caused by the effect of charges on coagulation and growth, which is not yet considered in any existing models and may be important in the stratosphere due to high ionization rates and the long lifetime of aerosols. Considering the importance of accurate PNSDs for projecting a realistic radiation

forcing response to stratospheric aerosol injection (SAI), it is essential to understand and incorporate such potentially important processes in SAI model simulations and to carry out further research to find out what other processes the present models might have missed.

1 Introduction

Solar radiation modification (also known as solar geoengineering) approaches are being developed in response to the climate crisis (IPCC, 2021). They would temporarily offset climate change by reducing incoming sunlight, augmenting (currently inadequate) mitigation efforts, and buying time to reduce atmospheric levels of CO_2, which is the root cause of the climate crisis. A recent report by the National Academies of Sciences, Engineering, and Medicine (NASEM) emphasizes the urgent need to have a comprehensive understanding of the feasibility and potential risks/benefits of solar climate intervention approaches (NASEM, 2021). Stratospheric aerosol injection (SAI) has demonstrated the most promise as proximately engineerable (Shepherd, 2009; Lockley et al., 2020; IPCC, 2021) and has been extensively studied using models (e.g., Geoengineering Model Intercomparison Project, GeoMIP: Kravitz et al., 2011; Geoengineering Large Ensemble, GLENS: Mills et al., 2017; Richter et al., 2022). The NASEM report (NASEM, 2021) pointed out that "the overall magnitude and spatial distribution of the forcing produced by SAI depends strongly on the aerosol size distribution" and "One of the research priorities for SAI is thus to address critical gaps in knowledge about the evolution of the aerosol particle size distribution". In the stratosphere, sulfate aerosols are formed by nucleation, followed by condensational growth and coagulation, and lost by evaporation in the upper stratosphere and downward sedimentation into the troposphere (Turco et al., 1982). New particle formation (NPF) (or nucleation) affects not only the number abundance but also the size distributions of stratospheric particles (e.g., Brock et al., 1995; Lee et al., 2003). There is increasing evidence (Weisenstein et al., 2022; Laakso et al., 2022) that the careful treatment of microphysical processes is necessary for projecting realistic radiative forcing responses to SAI.

The process of NPF under tropospheric conditions has been extensively explored over the last two decades through laboratory and field measurements, theoretical studies, and numerical simulations (e.g., Yu and Turco, 2000; Vehkamäki et al., 2002; Kulmala et al., 2004; Kirkby et al., 2011; Dawson et al., 2012; Zhang et al., 2012; Kürten et al., 2016; Yu et al., 2018; Kerminen et al., 2018; Lee et al., 2019). Although some of the advances in our understanding of nucleation gained in the last two decades can be applied to stratospheric conditions, focused studies specifically examining the mechanisms of NPF under stratospheric conditions are quite limited. Indeed, the H_2SO_4–H_2O binary homogenous nucleation (BHN) parameterization developed two decades ago by Vehkamäki et al. (2002) (named BHN_V2002 hereafter) has been widely used in SAI modeling studies when nucleation process is explicitly considered (e.g., Tilmes et al., 2015; Jones et al., 2021; Weisenstein et al., 2022). Tilmes et al. (2015) described a GeoMIP experiment designed for climate and chemistry models, using the stratospheric aerosol distribution derived from the ECHAM5-HAM microphysical model (Stier et al., 2005), which calculated nucleation rates with the BHN_V2002 scheme. Both models (UKESM1 and CESM2-WACCM6) employed for a recent GeoMIP G6sulfur study (Jones et al., 2021) used the BHN_V2002 scheme. In another recent SAI study based on three interactive stratospheric aerosol microphysics models (Weisenstein et al., 2022), two models (MAECHAM5-HAM and SOCOL-AER) used the BHN_V2002 scheme, while the other (CESM2-WACCM) used an empirical nucleation scheme to calculate nucleation rate as a function of sulfuric acid concentration only (i.e., no dependence on temperature and relative humidity). To our knowledge, the performance of this widely used BHN_V2002 under stratospheric conditions has not been carefully examined, probably due to the lack of suitable in situ measurements of freshly nucleated particles in the stratosphere for constraining the scheme. In this regard, particle size distributions down to 3 nm measured in situ during the NASA Atmospheric Tomography Mission (ATom) in the lowermost stratosphere (LMS) of both the Southern Hemisphere (SH) and Northern Hemisphere (NH) in four different seasons (Williamson et al., 2019, 2021; Kupc et al., 2020; Brock et al., 2021) provide much-needed data to constrain our understanding of the nucleation and particle microphysics in the stratosphere. In addition, well-controlled Cosmics Leaving OUtdoor Droplets (CLOUD) experiments taken under low temperature (within the range of stratosphere) can also be used to assess the performance of nucleation schemes under stratospheric conditions. Another important issue related to stratospheric particles is the role of ionization in nucleation. It is well established that nucleation of H_2SO_4–H_2O on ions is favored over homogenous nucleation (Hamill et al., 1982; Yu and Turco, 2000; Lovejoy et al., 2004; Kirkby et al. 2011; Yu et al., 2018), but the role of ionization in NPF in the stratosphere has not been considered in any previous SAI studies (to our knowledge) in spite of the very high ionization rates in the stratosphere.

In this study, we use both CLOUD laboratory measurements taken under very low stratospheric temperatures and ATom particle number size distribution (PNSD) measurements in the LMS to constrain nucleation mechanisms and model-simulated particle size distributions.

For three-dimensional simulation of size-resolved stratospheric aerosols, we use the GEOS-Chem with the unified tropospheric–stratospheric chemistry-transport model with the size-resolved advanced particle microphysics (APM) package.

2 Model and data

2.1 GEOS-Chem/APM

The GEOS-Chem model is a global three-dimensional model of atmospheric composition (e.g., Bey et al., 2001) and is continuously being improved (e.g., Luo et al., 2020; Holmes et al., 2019; Keller et al., 2014; Murray et al., 2012; Pye and Seinfeld, 2010; Van Donkelaar et al., 2008; Evans and Jacob, 2005; Martin et al., 2003). The GEOS-Chem tropospheric–stratospheric unified chemistry extension (UCX; Eastham et al., 2014), now the standard GEOS-Chem configuration, implements stratospheric chemistry, calculation of J values for shorter wavelengths, and improved modeling of high-altitude aerosols. Extension of the chemistry mechanism to include reactions relevant to the stratosphere enables the capturing of stratospheric responses and troposphere–stratosphere coupling. UCX adds 28 species and 104 kinetic reactions, including 8 heterogeneous reactions, along with 34 photolytic decompositions. Atomic oxygen (both $O(^3P)$ and $O(^1D)$) is explicitly modeled; although also of short lifetime in the stratosphere, these species are important in correctly modeling stratospheric chemistry. Photochemistry is extended up to the stratopause to high-energy photons (177 nm) using the Fast-JX model, which includes cross-section data for many species relevant to the troposphere and stratosphere. Photolysis rates respond to changes in the stratospheric ozone layer. Additional heterogeneous reactions (Kirner et al., 2011; Rotman et al., 2001; Shi et al., 2001) are included to capture seasonal ozone depletion. H_2O is treated as a chemically active advected tracer within the stratosphere. This permits chemical feedbacks between stratospheric ozone and aerosols and tropospheric photochemistry. The improved GEOS-Chem with coupled stratospheric–tropospheric responses has been evaluated with sonde and satellite measurements of O_3, HNO_3, H_2O, HCl, ClO, NO_2, and stratospheric intrusions (Eastham et al., 2014; Gronoff et al., 2021; Knowland et al., 2022). Yu and Luo (2009) incorporated a size-resolved (sectional) APM package into GEOS-Chem, henceforth referred to as GC–APM. The APM separates secondary particles from primary particles, uses 40 bins to represent secondary particles with high size resolution for the size range important for the growth of nucleated particles to accumulation mode sizes, and contains options to calculate nucleation rates based on different nucleation schemes. In GC–APM, nucleation is calculated before condensation using a time-splitting technique. Therefore, no competition between nucleation and condensation for sulfuric acid vapor is considered. In most conditions, nucleation consumes only a very small fraction ($< 1\,\%$) of sulfuric acid vapor in the air, and the time splitting does not affect the results. When the nucleation rate is high, a reduced time step for nucleation and growth is used to ensure that the fraction of sulfuric acid vapor consumed by nucleation each time step is small. The GC-APM uses a semi-implicit scheme to calculate sulfuric acid condensation together with sulfuric acid gas-phase production to ensure that the change of sulfuric acid vapor concentration is smooth. APM is fully coupled with GEOS-Chem in both the troposphere and stratosphere.

In the present study we have carried out GEOS–Chem–UCX/APM global simulations from January 2015 to May 2018, with the first 17 months as spin-up and the remaining period covering ATom 1–4 periods (June 2016–May 2018). The horizontal resolution is $4^\circ \times 5^\circ$, and there are 72 vertical layers. Emissions from different sources, regions, and species are computed via the Harvard–NASA Emissions Component (HEMCO) on a user-defined grid (Keller et al., 2014). Historical global anthropogenic emissions are based on the Community Emissions Data System (CEDS) inventory (Hoesly et al., 2018). Regional anthropogenic emissions over the United States, Canada, Europe, and East Asia are replaced by regional emission inventories of the National Emissions Inventory (NEI, https://www.epa.gov/air-emissions-inventories/2017-national-emissions-inventory-nei-data, last access: 30 June 2022), the Air Pollutant Emission Inventory (APEI, https://www.canada.ca/en/environment-climate-change/services/pollutants/air-emissions-inventory-overview.html, last access: 30 June 2022), the Co-operative Programme for Monitoring and Evaluation of the Long-range Transmission of Air Pollutants in Europe (EMEP, https://www.emep.int/index.html, last access: 30 June 2022), and the MIX Asian emission inventory (Li et al., 2017), respectively. Monthly mean aircraft emissions are generated based on the Aviation Emissions Inventory v2.0 (Stettler et al., 2011). The aircraft particle emissions include nucleation mode sulfate particles (emission index $= 2 \times 10^{17}$ per kilogram fuel, mean diameter $= 9$ nm, based on Kärcher et al., 2000), and black carbon and primary organic carbon (POC) particles. Global biomass burning is taken from the Global Fire Emissions Database version 4 (Van der Werf et al., 2017). The volcanic emissions of SO_2 are taken from AeroCom point-source data (Carn et al., 2015). Fixed global surface boundary conditions are applied for N_2O, CFCs, HCFCs, halons, OCS, and long-lived organic chlorine species (Eastham et al., 2014).

2.2 Airborne ATom measurements of PNSD

Measurements are essential in advancing our understanding of stratospheric aerosol properties and the fundamental processes governing these properties. NASA's Atmospheric Tomography Mission (ATom; Wofsy et al., 2021; Thompson et al., 2022) is a multi-agency effort that provides global in

situ aircraft observations of the vertical structure of aerosols from near surface to ∼ 12 km altitude. PNSDs are measured using the NOAA Aerosol Microphysical Properties (AMP) package (Brock et al., 2019), comprising nucleation-mode aerosol size spectrometer(s) (NMASS) (Williamson et al., 2018), ultra-high-sensitivity aerosol spectrometer(s) (UHSAS) (Kupc et al., 2018), and a laser aerosol spectrometer (LAS) covering aerosol sizes from 3 nm to 4.5 µm. The aerosol number abundance can be obtained by integrating the PNSD measurements.

2.3 The CLOUD (Cosmics Leaving OUtdoor Droplets) measurements

Laboratory measurements of nucleation rates as a function of key controlled parameters have been carried out in a 26.1 m^3 stainless steel cylinder chamber at the European Organization for Nuclear Research (CERN) in the framework of the Cosmics Leaving OUtdoor Droplets (CLOUD) experiment (e.g., Kirkby et al., 2011; Kürten et al., 2016; Dunne et al., 2016). Some of these experiments were conducted at the temperature in the range of those in the stratosphere (Kirkby et al., 2011; Dunne et al., 2016) which are used in this study to evaluate nucleation schemes under stratospheric conditions.

3 Results

3.1 H_2SO_4–H_2O binary homogeneous nucleation (BHN) and binary ion-mediated nucleation (BIMN) under stratospheric conditions

Nucleation is one of the microphysical processes influencing particle size distributions in the stratosphere (Turco et al., 1982). The CLOUD measurements under a wide range of well-controlled conditions (Kirkby et al., 2011; Dunne et al., 2016) provide a unique set of data to evaluate the nucleation theories. Yu et al. (2020) compared nucleation rates calculated based on a number of commonly used aerosol nucleation parameterizations with the CLOUD measurements. Here we specifically examine the comparison under stratospheric conditions where temperature is below ∼ 230 K. Since ammonia concentrations in the stratosphere are generally negligible, we focus on binary nucleation in the present study. The contribution of organics to particle formation, growth, and compositions in the upper troposphere and LMS has been investigated in several studies (Kupc et al., 2020; Murphy et al., 2021; Williamson et al., 2021). Because of the lack of information with regard to the low volatile gaseous organic species, the possible role of organics in new particle formation in LWS is not considered in the present study.

Figure 1 compares nucleation rates based on the following three different schemes with CLOUD measurements under stratospheric temperature range (T = 205–223 K): BHN of Vehkamäki et al. (2002) (BHN_V2002), BHN of Yu et al. (2020) (BHN_Y2020), and BIMN of Yu et al. (2020) (BIMN_Y2020). BHN_V2002 and BHN_Y2020 differ in terms of thermodynamic data and the nucleation approach used (Yu et al., 2020). To show the relative importance of homogeneous versus ion nucleation, BIMN rates at Q = 20 ion pairs cm^{-3} s^{-1} were given under the binary homogeneous condition in Fig. 1a, and BHN rates were also given under the binary ion nucleation condition in Fig. 1b. Nucleation rates based on BHN_V2002 are consistently 3–5 orders of magnitude higher than those observed under H_2SO_4–H_2O binary nucleation conditions without (Fig. 1a) and with (Fig. 1b) the effect of ionizations, while those based on BHN_Y2020 and BIMN_Y2020 are close to the observed values. It should be noted that similar to the CLOUD measurements with the effect of ionization, BHN rates are included in the BIMN rates (Yu et al., 2018), and the difference between BIMN and BHN rates indicates the contribution of ion-mediated or induced nucleation. Under the conditions of Fig. 1a, assuming an ionization rate of 20 ion pairs cm^{-3} s^{-1} (within the range of its typical value in the stratosphere), the BIMN rates are about 1 order of magnitude higher than the BHN rates when the nucleation rates are below ∼ 5 cm^{-3} s^{-1} but are close to BHN rates when nucleation rates are above ∼ 5 cm^{-3} s^{-1}. A similar difference between BHN_Y2020 and BIMN_Y2020 can also be seen in Fig. 1b, indicating the importance of ion nucleation at relatively lower nucleation rates (mostly associated with relatively lower H_2SO_4) and dominance of homogeneous nucleation at higher nucleation rates (associated with larger H_2SO_4). As we show next, H_2SO_4 in the background stratosphere is generally quite low and thus ion nucleation dominates, but BHN can become important in the SO_2 plumes injected into the stratosphere.

3.2 Nucleation rates and particle number concentrations in the stratosphere

Figure 2 shows the zonal mean SO_2 emission (SO_2_emit), particle number emitted by aviation (PN_aviation), temperature (T), relative humidity (RH), ionization rate (Q), and H_2SO_4 averaged during the 2-year period (June 2016–May 2018) covering ATom 1–4. To focus on the lower stratosphere (LS), only the values of these variables in the stratosphere (grid boxes with more than 50 % of time above the tropopause) are shown. The SO_2 emissions include all sources, including volcanos and aviation. During this period there was one relatively strong volcanic event, the Bezymianny volcano (55.98° N, 160.59° E), on 20 December 2017 that injected 5×10^6 kg S into an altitude of ∼ 14–18 km (Carn et al., 2015). Aviation emission is generally limited to below ∼ 12.5 km altitude. Based on the Modern-Era Retrospective analysis for Research and Applications, Version 2 (MERRA2) meteorology data, which are used to drive GEOS-Chem, almost all of the grid boxes at 12 km are under the tropopause in the tropics (30° N–30° S), most of the grid boxes at 12 km in the high-latitude regions (60–90° N,

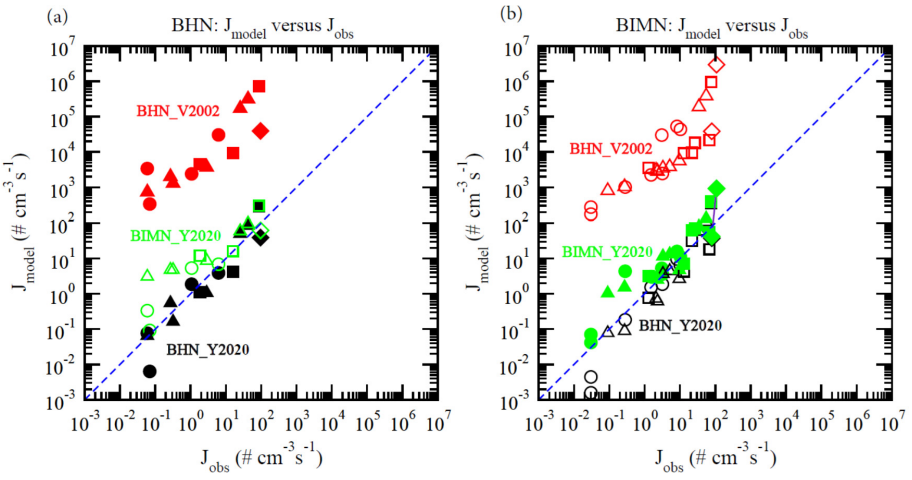

Figure 1. Comparison of nucleation rates based on three different schemes with CLOUD measurements within the low temperature range ($T = 205$–223 K) as that in the stratosphere for **(a)** binary homogeneous nucleation (no ionization) and **(b)** ion nucleation (at the presence of ionization rates 2.51–110 ion pairs cm^{-3} s^{-1}). The different nucleation schemes shown are BHN of Vehkamäki et al. (2002) (BHN_V2002), BHN of Yu et al. (2020) (BHN_Y2020), and BIMN of Yu et al. (2020) (BIMN_Y2020). For comparison, under the binary condition of panel **(a)**, BIMN rates at $Q = 20$ ion pairs cm^{-3} s^{-1} are given, while under the binary ion nucleation condition of panel **(b)**, BHN rates are also given. Values of H_2SO_4 vapor concentration ($[H_2SO_4]$) range from 10^6 to 3×10^7 cm^{-3} and are separated into four groups in the plots (circles: 10^6–5×10^6 cm^{-3}, triangles: 5×10^6–10^7 cm^{-3}, squares: 10^7–1.5×10^7 cm^{-3}, diamonds: 1.5×10^7–3×10^7 cm^{-3}).

60–90° S) are above the tropopause, and some fractions of the grid boxes at 12 km in the middle-latitude regions (30–60° N, 30–60° S) are above the tropopause. As can be seen from Fig. 2b, some of the aviation emissions in the middle- and high-latitude regions are in the LMS, and the amount emitted into the NH LMS is much higher (by several orders of magnitude) than that in the SH. The temperature in the LS ranges from 190–225 K, with the lowest value in the region just above the tropical tropopause (Fig. 2c). RH in the LS has the highest values near the tropopause but drops quickly with increasing altitude, from ∼ 30 %–50 % near the tropopause to ∼ 0.1 %–1 % at ∼ 25 km in the tropical and middle latitudes (Fig. 2d). The spatial variations of T and RH have important effects on nucleation in the LS. The cosmic-ray-induced ionization rate in the LS has a large latitudinal gradient, ranging from ∼ 40–100 ion pair std. cm^{-3} s^{-1} (here "std. cm^{-3}" refers to per cubic centimeter at standard temperature and pressure, 273 K and 1013 hPa) in the tropics to 100–400 ion pair std. cm^{-3} s^{-1} in the middle- and high-latitude region (Fig. 2e). The high ionization rates may have important implications for particle microphysics in the LS, which will also be discussed in Sect. 3.3. H_2SO_4 is the most important aerosol precursor in the LS, and its concentration depends on SO_2 concentrations and oxidation, condensation sink, and its vapor pressure that depends on T and RH. The annual mean H_2SO_4 (Fig. 2f) has large spatial variations, ranging from a minimum of ~ 1–2×10^5 std. cm^{-3} at altitudes of ∼ 12–15 km in polar regions to ~ 4–20×10^5 std. cm^{-3} close to the tropopause. From ∼ 18–25 km (well above the ATom measurement altitude), H_2SO_4 increases with altitude, mainly due to the increasing H_2SO_4 vapor pressure associated with vertical changes of T (Fig. 2c) and RH (Fig. 2d).

To demonstrate the effect of nucleation schemes on simulated aerosol properties, we compare in Fig. 3 zonal mean and vertical profiles of nucleation rates (J) and number concentrations of condensation nuclei larger than 3 nm (CN3), simulated based on the three nucleation schemes: BHN_V2002, BHN_Y2020, and BIMN_Y2020. In all three schemes, the aviation emissions of both SO_2 (Fig. 2a) and particle numbers (Fig. 2b) are the same. The model simulations indicate that NPF occurs in the lower stratosphere but is mostly confined to the LMS except in the area of volcano injection (for example, above ∼ 14 km around ∼ 52° N). There exist large differences in the nucleation rates predicted by the three schemes (noting the logarithmic color scale), with BHN_V2002 rates generally 1–4 orders of magnitude higher, while BIMN_Y2020 rates are ∼ 1 order of magnitude higher than those based on BHN-Y2020. The difference between BIMN_Y2020 and BHN_V2002 rates is smaller in the LMS over the tropics (30° S–30° N) where temperature is the lowest (see Fig. 2c). The magnitudes of differences are consistent with comparisons with CLOUD measurements (Fig. 1). The difference in nucleation rates leads to a substantial difference in CN3 in the LMS, with those based on BHN_V2002 a factor 2–5 higher than those based on BHN_Y2020 in the LMS. The LMS CN3 based on BIMN_Y2020 is about 50 % higher than that of BHN_Y2020. Compared to the difference in nucleation rates, the differences in CN3 are much smaller. This is expected, because on the one hand only a small fraction of nucleated particles survive the coagulation scavenging and grow beyond 3 nm, and on the other hand direct emission

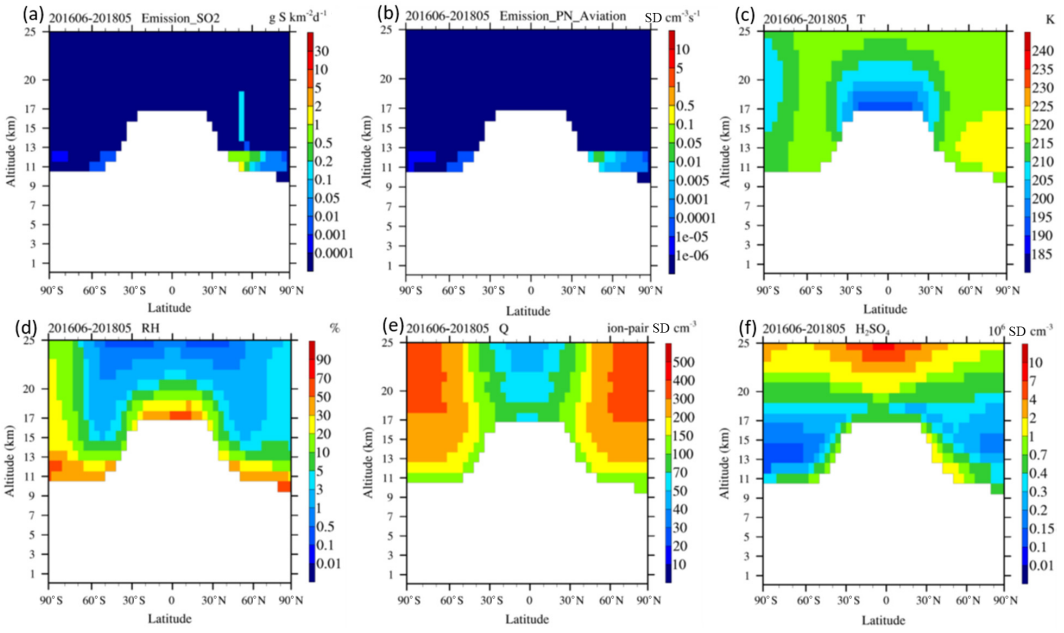

Figure 2. Zonal mean SO_2_emit, PN_Emit, T, RH, Q, and H_2SO_4 averaged during the 2-year period (June 2016–May 2018) covering ATom 1–4. To focus on the lower stratosphere, only the values of these variables in grid boxes with more than 50 % of time above the tropopause and below 25 km are shown.

of particle numbers from aviation (Fig. 2b; treated as direct emission but most of these are actually nucleated on chemiions in the exhaust plume shortly after emission) (Brock et al., 2000) and transport provides a substantial amount of CN3 even without nucleation. Nevertheless, nucleation is still significant enough to affect the CN3. It is interesting to note that CN3 based on BIMN_Y2020 is higher at altitudes $\gtrsim$ 22 km (Fig. 3h), which is associated with higher nucleation rates based on BIMN_Y2020, than those based on BHN_V2002 and BHN_Y2020 within the altitude range of 35–55 km. Another interesting point is that there is a much smaller vertical gradient in BHN_V2002 nucleation rates in the tropical region (30° S–30° N) within ∼ 17–20 km (see Fig. 3a and d), likely a result of different dependences of nucleation rates based on different schemes on T, RH, and H_2SO_4 which have large vertical variations (see Fig. 2). It can be seen from Fig. 3 that the simulations based on three nucleation schemes all show a large hemispheric difference in particle number concentrations (by a factor of ∼ 3–6) in the LMS at middle and high latitudes, consistent with the ATom measurements (Williamson et al., 2021). Our sensitivity study (by turning off aviation emission, not shown, to be reported in a separate study) indicates this large hemispheric difference is largely caused by aviation emissions, confirming the analysis of Williamson et al. (2021).

While it is difficult to observe nucleation rates in the stratosphere, the measurement of freshly nucleated nanoparticles can be used to constrain nucleation schemes. Figure 4a compares the model-simulated CN3 (all particles with a diameter larger than 3 nm, with the upper size limit of 12 µm corresponding to the size of the last model bin) based on the three nucleation schemes at altitudes of around 12 km in the SH at middle and high altitudes during four seasons with the corresponding ATom 1–4 observations. As an example, Fig. 4b–d shows the model-simulated horizontal distributions of CN3 at a 12 km altitude during ATom 4 with the values and locations of ATom 4 CN3 data overlaid. We choose the SH for comparison, as it represents the background stratosphere with minimum influence from anthropogenic emissions (i.e., aviation) (Fig. 2b), to avoid the uncertainty associated with aviation emissions. In Fig. 4, the model results are 2 months' average, corresponding to the flight months of each ATom campaign, while the measurement data points shown are those sampled within the altitude ranges of 11.5–12.5 km in the stratosphere (ozone > 250 ppbv and RH < 10 %, following the same stratosphere definitions as in Murphy et al. (2021) and Williamson et al., 2021) and averaged to a 4° × 5° grid box for comparison with modeled results. The impact of the nucleation scheme on CN3 can be clearly seen: BHN_V2002 overpredicted CN3 by a factor of 2–4, BHN_Y2020 slightly underpredicted CN3, and BIMN_Y2020 slightly overpredicted CN3. The larger vertical spread in CN3 from BHN_V2002 is caused by the large CN3 latitude gradient associated with higher nucleation near the tropopause (Fig. 3). The comparisons above show that the ATom measurements provide a good constraint on our understanding of the processes controlling CN3 in the LMS at middle and high latitudes.

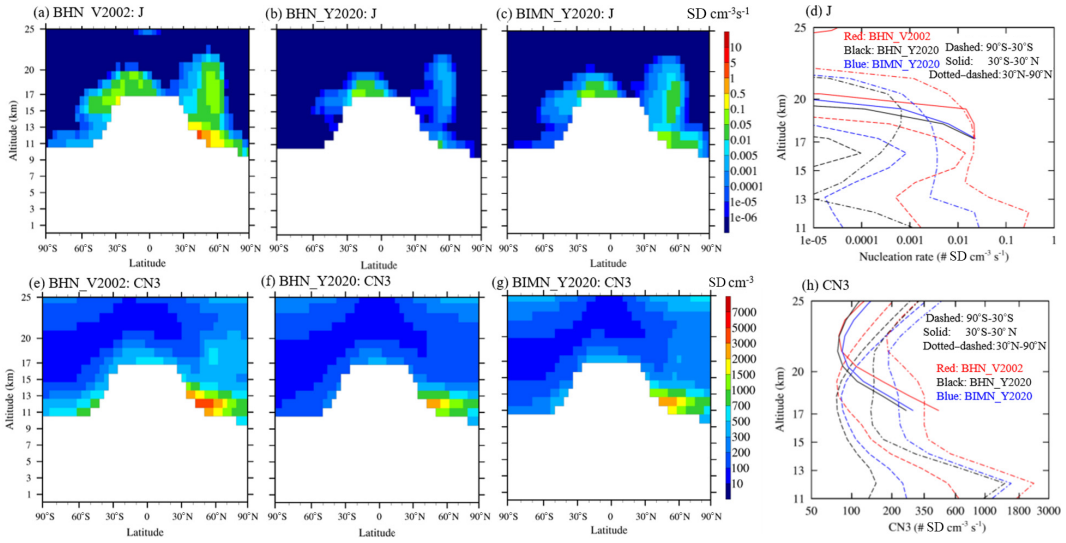

Figure 3. Model-simulated zonal mean and vertical profiles of nucleation rates (J, upper panels) and number concentrations of particles larger than 3 nm (CN3, lower panels) in the stratosphere during the 2-year period covering ATom 1–4 (June 2016–May 2018), based on three nucleation schemes (**a, e**: BHN_V2002, **b, f**: BHN_Y2020, and **c, g**: BIMN_Y2020). The vertical profiles in panels **(d)** and **(h)** are averaged for three latitude zones (90–30° S, 30° S–30° N, and 30–90° N). The values for those grids with at least 50 % of time above the tropopause are shown.

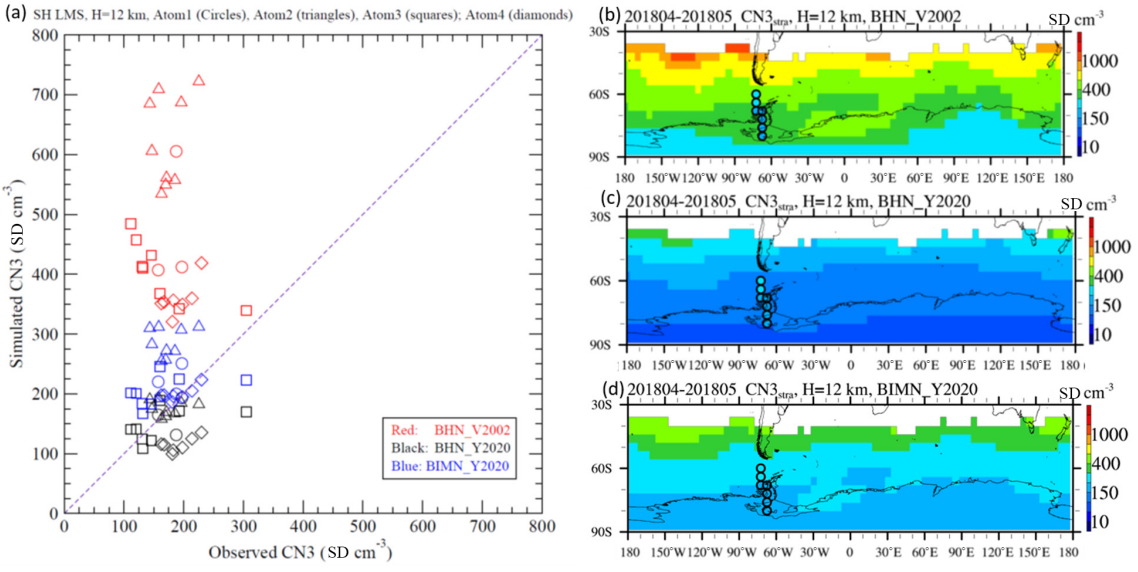

Figure 4. CN3 at altitudes of around 12 km in the SH at middle and high latitudes: **(a)** model-simulated versus observed during ATom 1–4 (circles: ATom1, triangles: ATom2, squares: ATom3, diamonds: ATom4) and **(b–d)** model-simulated horizontal distributions corresponding to ATom 4 based on three different nucleation schemes (BHN_V2002, BHN_Y2020, and BIMN_Y2020), with the values and locations of ATom 4 CN3 measurements shown in the circles.

3.3 PNSDs in the stratosphere

Figure 5 shows the model-simulated evolution of PNSDs at an altitude of 12 km over a site in the SH (70° S, 60° W) during the 2-year ATom period based on the three different nucleation schemes. The PNSDs shown in Fig. 5 are averaged into four different seasons corresponding to the months of ATom 1–4 field campaigns and are presented in Fig. 6 for comparison with the observed mean PNSDs in the SH LMS (Williamson et al., 2021). It should be noted that modeled PNSDs in Fig. 6 are 2 months' average at one fixed site at an altitude of 12 km (in the region where many of the SH LMS measurements were taken, see Fig. 4), while the observed ones are averaged over all SH LMS air mass sampled during the corresponding ATom campaign. While the compari-

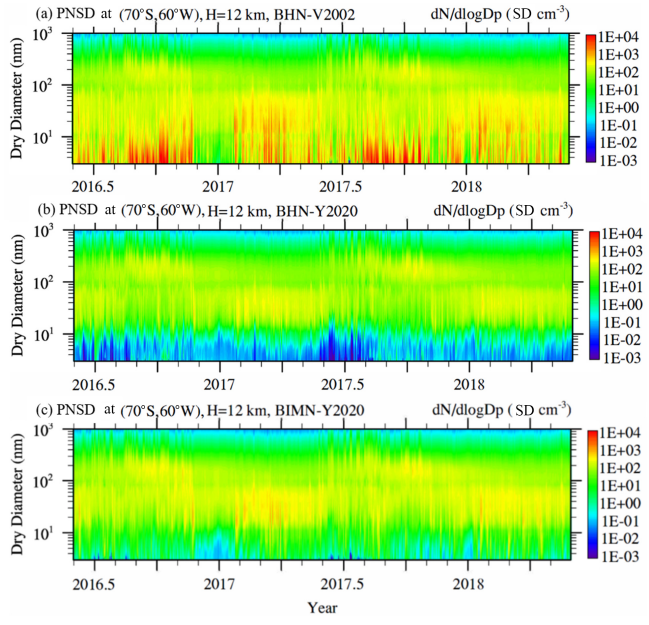

Figure 5. Model-simulated evolution of PNSDs at a site in the SH (70° S, 60° W) at an altitude of 12 km based on three nucleation schemes (BHN_2002, BHN_Y2020, and BIMN_Y2020).

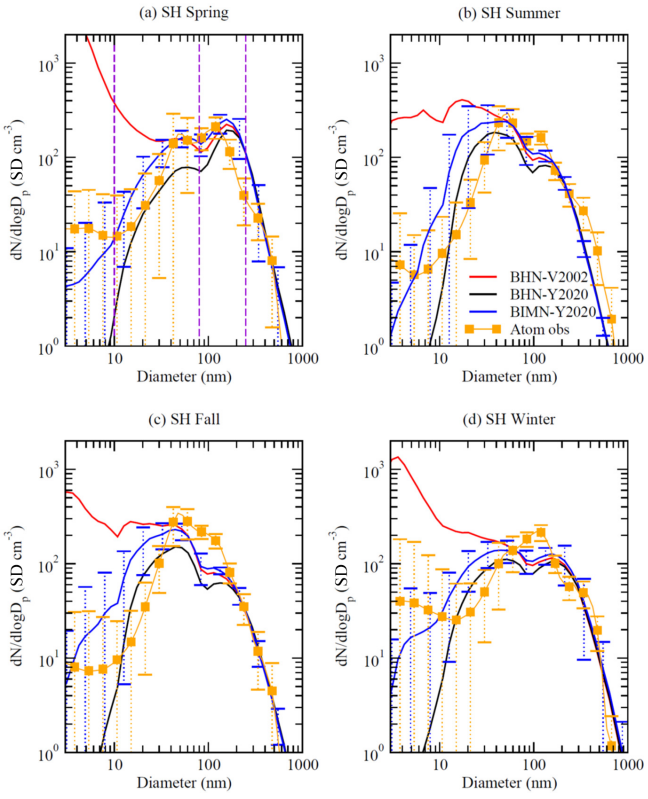

Figure 6. Model-simulated seasonal mean PNSDs at a site in the SH (70° S, 60° W) at an altitude of 12 km based on three nucleation schemes and comparisons with the corresponding ATom measurements (**a**: SH spring in September–October 2017, **b**: SH summer in January–February 2017, **c**: SH fall in April–May 2018, and **d**: SH winter in June–July 2016). To take into account the variations in both model and observed PNSDs, standard deviations are shown as error bars in the measured and modeled curves based on BIMN_Y2020. Three vertical dashed lines at 10, 80, and 250 nm are drawn in **(a)** to guide the eye to the four modes discussed in the text.

son in Fig. 6 is not exactly coterminous, it allows us to make quantitative comparisons of modeled and observed PNSDs. To take into account the variations in both model and observed PNSDs, standard deviations are shown as error bars in the measured and modeled curves based on BIMN_Y2020.

Figure 6 shows that PNSDs measured in the background LMS have multiple modes: a nucleation mode (NuclM: 10 nm), an Aitken mode (AitkenM: ∼10–80 nm), and two accumulation modes (AccuM1: ∼80–250 nm and AccuM2: ∼250–700 nm). It should be noted that these modes are not the same size limits as those presented in the public ATom dataset. As shown in Figs. 5 and 6, the model based on all three nucleation schemes generally captures the AitkenM and AccuM1 and the existence of a minimum in PNSDs around 80 nm, although there exist differences. Interestingly, the relative height (or peak values of dN/dlogD$_p$) of AitkenM and AccuM1 has strong seasonal variations. The model captures a relatively higher AitkenM in the SH summer and fall and a higher AccuM1 in the SH spring. The model-simulated PNSDs also agree well with the measurements in terms of the size-dependent normalized standard deviation (σ_N, i.e., the standard deviation σ divided by the mean): a relatively smaller σ_N for AccuM1 and a larger size part of AitkenM and a much larger σ_N for NuclM, a smaller size part of AitkenM and AccuM2. While the larger σ_N for NuclM is understandable because of NPF, it is surprising for AccuM2. The AccuM2 particles have relatively long lifetimes and are expected to be well-mixed (and thus have small variations) in the LS. The transport of AccuM2 particles from the upper troposphere (UT) may contribute to the larger variations. Murphy et al. (2021) showed the chemical signature of this transported mode, and here we show that the variation in the size distribution may also contain information about the mixing of UT particles into the LMS. Compared to the observations, the model-simulated AccuM2 σ_N are larger in the SH winter and spring but are smaller in the SH summer and fall. The possible reasons for the large variations of AccuM2 in the LMS and the differences between model simulations and measurements remain to be studied.

The large impacts of nucleation schemes on PNSDs, especially those smaller than 100 nm, can be seen in Fig. 6. The formation rates and concentrations of nucleation mode particles are very high based on BHN_V2002 (peak $dN/d\log D_p$ values reaching well above 10^3 std. cm^{-3}), negligible based on BHN_Y2020 ($dN/d\log D_p$ values for particles < 10 nm are generally below 1 std. cm^{-3}), and moderate based on BIMN_Y2020. When compared to the observed values, the

number concentrations of particles within 3–10 nm based on BHN_V2002 are 1–2 orders of magnitude too high, but those based on BHN_Y2020 are 1–2 orders of magnitudes too low, while those based on BIMN_Y2020 are of the same order of magnitude. The impact of nucleation schemes on NuclM propagates into the AitkenM and AccuM1, with BHN_Y2020 giving the lowest number concentrations, while BHN_V2002 gives the highest AitkenM and BIMN_Y2020 gives the highest AccuM1. It should be noted that, while the line of BHN-Y2020 is lower than that of BIMN and BHN-V2002 for particles of smaller sizes ($\lesssim$ 300 nm), it is slightly higher for larger particles ($\gtrsim$ 300 nm). This is consistent with the competition of sulfuric acid gas between pre-existing larger particles and nucleated smaller particles. It is interesting to note that AccuM1 based on BIMN_Y2020 is higher than that based on BHN_V2002, although BHN_V2002 predicts higher NuclM and AitkenM, indicating a non-linear interaction among nucleation, growth, and coagulation. The competition between nucleation and condensation for available sulfuric acid gas has been shown to be important for SAI studies (Laakso et al., 2022).

There exists a number of differences in the simulated and observed PNSDs. Firstly, measurements indicate a slight increase of $\mathrm{d}N/\mathrm{d}\log D_\mathrm{p}$ with decreasing sizes for particles < 10 nm but the simulated PNSDs based on BIMN_Y2020, the scheme is mostly consistent with CLOUD measurements and predicting NuclM concentrations closest to those observed, and decreases with decreasing sizes for particles < 10 nm. The possible reasons of the difference remain to be investigated but are probably associated with uncertainty in nucleation rates and size-dependent growth rates of freshly nucleated particles, and/or the fact that ATom observations are biased towards daytime. In addition, the small number of particles in this mode is likely within the uncertainty in the ATom measurements (about 7 % of the total number of particles) so that this measured mode may not be significant. Secondly, the model appears to overpredict the smaller size part ($\sim$ 10–40 nm) of AitkenM, although it is close to the larger part of the mode ($\sim$ 40–80 nm). The overprediction may be a result of the underestimated growth rates, coagulation scavenging rates of these particles, or overpredicted growth rates of NuclM particles. Thirdly, the model generally overpredicts the mean mode sizes of AccuM1 and underpredicts the concentrations of the mode except in the SH spring. The nucleation schemes have observable effects on the concentrations and mean sizes of AccuM1, and overall the simulations based on BIMN_Y2020 are in stronger agreement with measurements. Finally, the observed PNSDs show a clear AccuM2 in all seasons except fall, but such a mode cannot be clearly seen in the model-simulated PNSDs, indicating that the model underpredicts the concentrations of AccuM2 mode particles. AccuM2 particles are within the size range with the most efficient scattering of solar radiation and thus are important for SAI. It is therefore necessary to identify the sources of this difference and to improve the model.

As pointed out earlier, the comparison in Fig. 6 does not exactly match in terms of time and location, which likely contributes to some of the differences shown in Fig. 6. Some of the differences can also be caused by the uncertainties in the model in terms of emissions, transport, chemistry, aerosol microphysics, and deposition. Nevertheless, some of these differences, especially the shape of PNSDs (AccuM2, NuclM, etc.), are unlikely to be fully accounted for by the above-mentioned possible mismatch or model uncertainties and thus may indicate that some fundamental processes are not represented in the model. One possible cause of the differences is that the transport of organic sulfate particles from the UT (Murphy et al., 2014, 2021) is not properly simulated by the model. Based on size-resolved particle composition measurements, Murphy et al. (2021) showed that the LMS accumulation mode particles (diameter $\sim$ 0.1 and 1.0 µm) have at least two modes: the larger mode consists mostly of sulfuric acid particles produced in the stratosphere, and the smaller mode consists mostly of organic sulfate particles transported from the troposphere. Murphy et al. (2014) showed that the fraction of organic sulfate aerosols above the tropopause decreases quickly with altitudes. While the organic sulfate mode aerosols from the UT may contribute to the bimodal structure of accumulation mode particles in the LMS observed during ATom, it is unlikely to contribute to the bimodal structure of particles larger than $\sim$ 200 nm observed at an altitude above $\sim$ 20 km both in the background and in volcano-perturbed stratosphere (Deshler et al., 2003, 2019; also see Fig. 7). Here, we suggest that the role of charges on coagulation and growth of particles in the stratosphere could be another process causing the bimodal of large particles in the stratosphere.

As shown Fig. 2e, ionization rates are high in the LS, ranging from $\sim$ 40–100 ion pair std. $\mathrm{cm}^{-3}\,\mathrm{s}^{-1}$. Due to their low number concentrations ($\sim$ 100–1000 std. cm^{-3}) but long lifetime, particles in the stratosphere are expected to be in charge equilibrium. Figure 7 shows the mean particle number size distribution (PNSD) and particle volume size distribution (PVSD) observed during ATom 1–4 in the SH LMS and measured within a 20–25 km altitude over Laramie, WY, in 1992 and the fraction of particles carrying n charges based on the modified Boltzmann equilibrium equation (Clement and Harrison, 1992). The bimodal structure of accumulation mode particles can be clearly seen in both the background and volcano-perturbed stratosphere. It should be noted that while the smaller mode generally dominates the number concentrations, the larger mode dominates mass concentrations. Under equilibrium more particles are charged (i.e., $1 - f_0 > 50\,\%$) than neutral (f_0) for particles with a diameter larger than $\sim$ 80 nm and a significant fraction (> 25 %) of particles larger than 300 nm carrying multiple charges. While the equilibrium charge fraction is small for NuclM particles ($\lesssim$ 10 nm), this fraction can be much larger when nucleation on ions occurs, which is consistent with the observed overcharging of freshly nucleated particles (Laakso

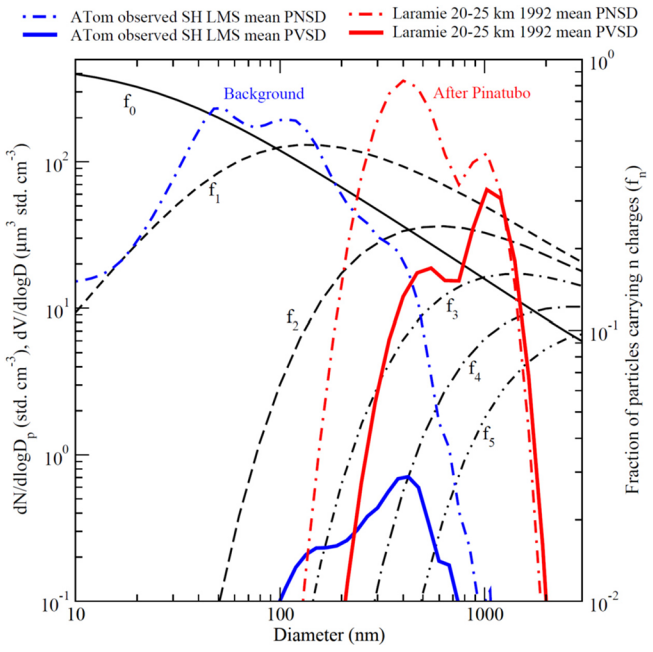

Figure 7. ATom 1–4 mean observed particle number size distribution (PNSD or $\mathrm{d}N/\mathrm{d}\log D_\mathrm{p}$) and particle volume size distribution (PVSD or $\mathrm{d}V/\mathrm{d}\log D_\mathrm{p}$) in the SH LMS, balloon-borne measured mean PNSD and PVSD within a 20–25 km altitude over Laramie, WY, in 1992, and fraction of particles carrying n ($n = 0$, 1, 2, 3, 4, and 5) charges based on the modified Boltzmann equilibrium equation (Clement and Harrison, 1992). Note that f_n with $n \geq 1$ includes both positive and negative charges, i.e., half of f_1 carries one negative charge, while the other half carries one positive charge.

et al., 2007; Yu and Turco, 2008). Particle coagulation rates are influenced by forces exerted between colliding particles, including Van der Waals and electrostatic forces, which can modify the effective collision cross section and sticking coefficient. The Van der Waals force has been shown to be important in the stratosphere (English et al., 2011, 2012) and has been considered in the simulations shown above. The effects of charges on coagulation and implications for PNSDs in the stratosphere have not been studied yet (to our knowledge). Since coagulation is a dominant process for the growth of accumulation mode particles in the stratosphere, we hypothesize that differential coagulation rates for neutral and charged particles in accumulation modes can potentially act as a physical process separating the modeled single accumulation mode (Fig. 6) into two modes (AccuM1 and AccuM2) as observed. Further research is needed to test this hypothesis. In addition to affecting coagulation, charge on small particles can also enhance the growth rate due to ion–dipole interactions of condensing molecules with charged particles (Nadykto and Yu, 2005). This enhancement is expected to be stronger in the stratosphere because of lower temperature (Nadykto and Yu, 2005). Beside these, Svensmark et al. (2020) showed that the condensation of ion clusters can enhance particle growth rates. How much the enhanced coagulation and growth rates of charged particles may shape PNSDs and modes in the stratosphere remains to be investigated.

4 Summary and discussions

Interest in stratospheric aerosols has been increasing in recent years, due to the ongoing discussion about the plausibility, potential benefits, and risks of offsetting climate change through stratospheric aerosol injection (SAI) to buy time for the reduction of CO_2 in the atmosphere. Recent studies indicate the dependence of SAI radiative efficacy (Dai et al., 2018) on the particle size distribution (NASEM, 2021), and thus it is critical to improve the foundational understanding and model representation of aerosol microphysics processes controlling the evolution of stratospheric aerosols, both under background conditions and perturbed scenarios. While formation and growth of particles in the troposphere have been extensively studied in the past two decades, very limited efforts have been devoted to understanding these in the stratosphere.

In the present study we use both CLOUD laboratory measurements taken under very low stratospheric temperatures and ATom in situ observations of particle number size distributions (PNSDs) down to 3 nm to constrain nucleation schemes and model-simulated particle size distributions in the lowermost stratosphere (LMS). We show that the binary homogenous nucleation scheme used in most of the existing SAI modeling studies overpredicts the nucleation rates by 3–4 orders of magnitude (when compared to CLOUD data), leading to significant overprediction of particle number concentrations in the background stratosphere (by a factor of 2–4 in the SH LMS compared to ATom data). Based on a recently developed kinetic nucleation model which provides rates of both ion-mediated nucleation (IMN) and BHN at low temperatures in good agreement with CLOUD measurements, both BHN and IMN occur in the stratosphere, but IMN rates are generally more than 1 order of magnitude higher than BHN rates and thus dominate nucleation in the background stratosphere.

In the SH LMS that has minimal influences from anthropogenic emissions, our analysis shows that ATom-measured PNSDs generally have four apparent modes: a nucleation mode (NuclM: 10 nm), which may not be statistically significant; an Aitken mode (AitkenM: ∼ 10–80 nm); and two accumulation modes (AccuM1: ∼ 80–250 nm and AccuM2: ∼ 250–700 nm). The model generally captures the AitkenM and AccuM1 and the existence of a minimum in PNSDs at ∼ 80 nm, although there are differences. The model captures a relatively higher AitkenM in the SH summer and fall and a higher AccuM1 in the SH spring. The model-simulated PNSDs also agree well with the measurements in terms of the size-dependent standard deviations: relatively smaller stan-

dard deviations for AccuM1 and larger size parts of AitkenM and much larger standard deviations for NuclM and smaller size parts of AitkenM and AccuM2.

A detailed comparison indicates the existence of a third PNSD mode peaking around 300–400 nm in the ATom measurements that are not captured by the model. Compared to the observations, the model-simulated AccuM2 standard deviations are larger in the SH winter and spring but are smaller in the SH summer and fall. In addition, the model overpredicts the number concentration of particles in the size range of 10–50 nm. These differences may indicate that, in addition to nucleation, the model may be missing some fundamental microphysical processes of stratospheric aerosols. Our analysis shows that, in the stratosphere, more particles are charged (positive + negative) than neutral for particles with a diameter larger than ~ 80 nm and a significant fraction ($> 25\,\%$) of particles larger than 300 nm carrying multiple charges. We propose that the role of charges on the coagulation and growth of particles in the stratosphere, where ionization rates are high and particles have very long lifetimes, is likely one of such processes. Considering the importance of accurate particle size distributions (especially the accumulation mode particles) for projecting a realistic radiative forcing response to stratospheric aerosols, it is essential to understand and incorporate such potentially important processes in model simulations of future changes in the stratosphere. It should be noted that the ATom measurement period does not have a high stratospheric aerosol loading (i.e., no major volcano eruptions). It remains to be investigated if previous assessments of volcanic aerosol microphysics missed something important. We expect the uncertainties in the nucleation schemes and unknown cause of the bimodal structure of accumulation mode particles will affect particle optical properties and surface area and thus radiative forcing or chemistry. In addition to what we have shown in this study, there are likely other uncertainties or missing processes we do not know, and the community needs to identify and resolve these. The present work highlights the importance of advancing scientific understanding of processes controlling properties of stratospheric particles; identifying important processes that the present models might have missed; and further development, improvement, and validation of models for reducing uncertainties of SAI simulations (e.g., Golja et al., 2021; Sun et al., 2022).

Code and data availability. The GEOS-Chem model is available to the public at https://doi.org/10.5281/zenodo.3507501 (The International GEOS-Chem User Community, 2019). Simulation output in this analysis is available at https://doi.org/10.5281/zenodo.6909944 (Yu, 2022). The ATom dataset is available at https://daac.ornl.gov/ATOM/campaign/ (last access: 30 June 2022; Wofsy et al., 2021).

Author contributions. FY designed the research. GL, SE, and FY developed the model. CJW, AK, and CAB collected the ATom data. FY and AAN performed the data analysis and prepared the paper. All co-authors contributed to the interpretation of the results, as well as paper review and editing.

Competing interests. The contact author has declared that none of the authors has any competing interests.

Disclaimer. Publisher's note: Copernicus Publications remains neutral with regard to jurisdictional claims in published maps and institutional affiliations.

Acknowledgements. The MERRA-2 data used in this study have been provided by the Global Modeling and Assimilation Office (GMAO) at NASA's Goddard Space Flight Center. The authors acknowledge the National Aeronautics and Space Administration (NASA) and SilverLining for funding.

Financial support. This research has been supported by the National Aeronautics and Space Administration (grant nos. 80NSSC19K1275 and 80NSSC21K1199) and SilverLining.

Review statement. This paper was edited by Andreas Petzold and reviewed by three anonymous referees.

References

Bey, I., Jacob, D. J., Yantosca, R. M., Logan, J. A., Field, B. D., Fiore, A. M., Li, Q., Liu, H. Y., Mickley, L. J., and Schultz, M. G.: Global modeling of tropospheric chemistry with assimilated meteorology: Model description and evaluation, J. Geophys. Res.-Atmos., 106, 23073–23095, https://doi.org/10.1029/2001JD000807, 2001.

Brock, C. A., Hamill, P., Wilson, J. C., Jonsson, H. H., and Chan, K. R.: Particle formation in the upper tropical troposphere – A source of nuclei for the stratospheric aerosol, Science, 270, 1650–1653, https://doi.org/10.1126/science.270.5242.1650, 1995.

Brock, C. A., Schröder, F., Kärcher, B., Petzold, A., Busen, R., and Fiebig, M.: Ultrafine particle size distributions measured in aircraft exhaust plumes, J. Geophys. Res.-Atmos., 105, 26555–26567, https://doi.org/10.1029/2000jd900360, 2000.

Brock, C. A., Williamson, C., Kupc, A., Froyd, K. D., Erdesz, F., Wagner, N., Richardson, M., Schwarz, J. P., Gao, R.-S., Katich, J. M., Campuzano-Jost, P., Nault, B. A., Schroder, J. C., Jimenez, J. L., Weinzierl, B., Dollner, M., Bui, T., and Murphy, D. M.: Aerosol size distributions during the Atmospheric Tomography Mission (ATom): methods, uncertainties, and data products, Atmos. Meas. Tech., 12, 3081–3099, https://doi.org/10.5194/amt-12-3081-2019, 2019.

Brock, C. A., Froyd, K. D., Dollner, M., Williamson, C. J., Schill, G., Murphy, D. M., Wagner, N. J., Kupc, A., Jimenez, J. L.,

Campuzano-Jost, P., Nault, B. A., Schroder, J. C., Day, D. A., Price, D. J., Weinzierl, B., Schwarz, J. P., Katich, J. M., Wang, S., Zeng, L., Weber, R., Dibb, J., Scheuer, E., Diskin, G. S., DiGangi, J. P., Bui, T., Dean-Day, J. M., Thompson, C. R., Peischl, J., Ryerson, T. B., Bourgeois, I., Daube, B. C., Commane, R., and Wofsy, S. C.: Ambient aerosol properties in the remote atmosphere from global-scale in situ measurements, Atmos. Chem. Phys., 21, 15023–15063, https://doi.org/10.5194/acp-21-15023-2021, 2021.

Carn, S. A., Yang, K., Prata, A. J. and Krotkov, N. A.: Extending the long-term record of volcanic SO_2 emissions with the Ozone Mapping and Profiler Suite nadir mapper, Geophys. Res. Lett., 42, 925–932, https://doi.org/10.1002/2014GL062437, 2015.

Clement, C. F. and Harrison, R. G.: The charging of radioactive aerosols, J. Aerosol Sci., 23, 481–504, https://doi.org/10.1016/0021-8502(92)90019-R, 1992.

Dai, Z., Weisenstein, D. K., and Keith, D. W.: Tailoring meridional and seasonal radiative forcing by sulfate aerosol solar geoengineering, Geophys. Res. Lett., 45, 1030–1039, https://doi.org/10.1002/2017GL076472, 2018.

Dawson, M. L., Varner, M. E., Perraud, V., Ezell, M. J., Gerber, R. B., and Finlayson-Pitts, B. J.: Simplified mechanism for new particle formation from methanesulfonic acid, amines, and water via experiments and ab initio calculations, P. Natl. Acad. Sci. USA, 109, 18719–18724, 2012.

Deshler, T., Hervig, M. E., Hofmann, D. J., Rosen, J. M., and Liley, J. B.: Thirty years of in situ stratospheric aerosol size distribution measurements from Laramie, Wyoming (41°N), using balloon-borne instruments, J. Geophys. Res.-Atmos., 108, 4167, https://doi.org/10.1029/2002JD002514, 2003.

Deshler, T., Luo, B., Kovilakam, M., Peter, T., and Kalnajs, L. E.: Retrieval of Aerosol Size Distributions From In Situ Particle Counter Measurements: Instrument Counting Efficiency and Comparisons With Satellite Measurements, J. Geophys. Res.-Atmos., 124, 5058–5087, https://doi.org/10.1029/2018JD029558, 2019.

Dunne, E. M., Gordon, H., Kürten, A., Almeida, J., Duplissy, J., Williamson, C., Ortega, I. K., Pringle, K. J., Adamov, A., Baltensperger, U., Barmet, P., Benduhn, F., Bianchi, F., Breitenlechner, M., Clarke, A., Curtius, J., Dommen, J., Donahue, N. M., Ehrhart, S., Flagan, R. C., Franchin, A., Guida, R., Hakala, J., Hansel, A., Heinritzi, M., Jokinen, T., Kangasluoma, J., Kirkby, J., Kulmala, M., Kupc, A., Lawler, M. J., Lehtipalo, K., Makhmutov, V., Mann, G., Mathot, S., Merikanto, J., Miettinen, P., Nenes, A., Onnela, A., Rap, A., Reddington, C. L. S., Riccobono, F., Richards, N. A. D., Rissanen, M. P., Rondo, L., Sarnela, N., Schobesberger, S., Sengupta, K., Simon, M., Sipilä, M., Smith, J. N., Stozkhov, Y., Tomé, A., Tröstl, J., Wagner, P. E., Wimmer, D., Winkler, P. M., Worsnop, D. R., and Carslaw, K. S.: Global particle formation from CERN CLOUD measurements, Science, 354, 1119–1124, https://doi.org/10.1126/science.aaf2649, 2016.

Eastham, S. D., Weisenstein, D. K., and Barrett, S. R.: Development and evaluation of the unified tropospheric–stratospheric chemistry extension (UCX) for the global chemistry-transport model GEOS-Chem, Atmos. Environ., 89, 52–63, 2014.

English, J. M., Toon, O. B., Mills, M. J., and Yu, F.: Microphysical simulations of new particle formation in the upper troposphere and lower stratosphere, Atmos. Chem. Phys., 11, 9303–9322, https://doi.org/10.5194/acp-11-9303-2011, 2011.

English, J. M., Toon, O. B., and Mills, M. J.: Microphysical simulations of sulfur burdens from stratospheric sulfur geoengineering, Atmos. Chem. Phys., 12, 4775–4793, https://doi.org/10.5194/acp-12-4775-2012, 2012.

Evans, M. J. and Jacob, D. J.: Impact of new laboratory studies of N_2O_5 hydrolysis on global model budgets of tropospheric nitrogen oxides, ozone, and OH, Geophys. Res. Lett., 32, L09813, https://doi.org/10.1029/2005GL022469, 2005.

Golja, C. M., Chew, L. W., Dykema, J. A., and Keith, D. W.: Aerosol dynamics in the near field of the SCoPEx stratospheric balloon experiment, J. Geophys. Res.-Atmos., 126, e2020JD033438, https://doi.org/10.1029/2020JD033438, 2021.

Gronoff, G., Berkoff, T., Knowland, K. E., Lei, L., Shook, M., Fabbri, B., Carrion, W., and Langford, A. O.: Case study of stratospheric Intrusion above Hampton, Virginia: lidar-observation and modeling analysis, Atmos. Environ., 259, 118498, https://doi.org/10.1016/j.atmosenv.2021.118498, 2021.

Hamill, P., Turco, R. P., Kiang, C. S., Toon, O. B., and Whitten, R. C.: An analysis of various nucleation mechanisms for sulfate particles in the stratosphere, J. Aerosol Sci., 13, 561–585, 1982.

Hoesly, R. M., Smith, S. J., Feng, L., Klimont, Z., Janssens-Maenhout, G., Pitkanen, T., Seibert, J. J., Vu, L., Andres, R. J., Bolt, R. M., Bond, T. C., Dawidowski, L., Kholod, N., Kurokawa, J.-I., Li, M., Liu, L., Lu, Z., Moura, M. C. P., O'Rourke, P. R., and Zhang, Q.: Historical (1750–2014) anthropogenic emissions of reactive gases and aerosols from the Community Emissions Data System (CEDS), Geosci. Model Dev., 11, 369–408, https://doi.org/10.5194/gmd-11-369-2018, 2018.

Holmes, C. D., Bertram, T. H., Confer, K. L., Graham, K. A., Ronan, A. C., Wirks, C. K., and Shah, V.: The role of clouds in the tropospheric NO_x cycle: A new modeling approach for cloud chemistry and its global implications, Geophys. Res. Lett., 46, 4980–4990, 2019.

IPCC: Climate Change 2021: The Physical Science Basis. Contribution of Working Group I to the Sixth Assessment Report of the Intergovernmental Panel on Climate Change, edited by: Masson-Delmotte, V., Zhai, P., Pirani, A., Connors, S. L., Péan, C., Berger, S., Caud, N., Chen, Y., Goldfarb, L., Gomis, M. I., Huang, M., Leitzell, K., Lonnoy, E., Matthews, J. B. R., Maycock, T. K., Waterfield, T., Yelekçi, O., Yu, R., and Zhou, B., Cambridge University Press, 2021.

Jones, A., Haywood, J. M., Jones, A. C., Tilmes, S., Kravitz, B., and Robock, A.: North Atlantic Oscillation response in GeoMIP experiments G6solar and G6sulfur: why detailed modelling is needed for understanding regional implications of solar radiation management, Atmos. Chem. Phys., 21, 1287–1304, https://doi.org/10.5194/acp-21-1287-2021, 2021.

Kärcher, B., Turco, R. P., Yu, F., Danilin, M. Y., Weisenstein, D. K., Miake-Lye, R. C., and Busen, R.: A unified model for ultrafine aircraft particle emissions, J. Geophys. Res.-Atmos., 105, 29379–29386, 2000.

Keller, C. A., Long, M. S., Yantosca, R. M., Da Silva, A. M., Pawson, S., and Jacob, D. J.: HEMCO v1.0: a versatile, ESMF-compliant component for calculating emissions in atmospheric models, Geosci. Model Dev., 7, 1409–1417, https://doi.org/10.5194/gmd-7-1409-2014, 2014.

Kerminen, V. M., Chen, X., Vakkari, V., Petäjä, T., Kulmala, M., and Bianchi, F.: Atmospheric new particle formation and growth: review of field observations, Environ. Res. Lett., 13, 103003, https://doi.org/10.1088/1748-9326/aadf3c, 2018.

Kirkby, J., Curtius, J., Almeida, J., Dunne, E., Duplissy, J., Ehrhart, S., Franchin, A., Gagné, S., Ickes, L., Kürten, A., Kupc, A., Metzger, A., Riccobono, F., Rondo, L., Schobesberger, S., Tsagkogeorgas, G., Wimmer, D., Amorim, A., Bianchi, F., Breitenlechner, M., David, A., Dommen, J., Downard, A., Ehn, M., Flagan, R. C., Haider, S., Hansel, A., Hauser, D., Jud,W., Junninen, H., Kreissl, F., Kvashin, A., Laaksonen, A., Lehtipalo, K., Lima, J., Lovejoy, E. R., Makhmutov, V., Mathot, S., Mikkilä, J., Minginette, P., Mogo, S., Nieminen, T., Onnela, A., Pereira, P., Petäjä, T., Schnitzhofer, R., Seinfeld, J. H., Sipilä, M., Stozhkov, Y., Stratmann, F., Tomé, A., Vanhanen, J., Viisanen, Y., Vrtala, A., Wagner, P. E., Walther, H., Weingartner, E., Wex, H., Winkler, P. M., Carslaw, K. S., Worsnop, D. R., Baltensperger, U., and Kulmala, M.: The role of sulfuric acid, ammonia and galactic cosmic rays in atmospheric aerosol nucleation, Nature, 476, 429–433, 2011.

Kirner, O., Ruhnke, R., Buchholz-Dietsch, J., Jöckel, P., Brühl, C., and Steil, B.: Simulation of polar stratospheric clouds in the chemistry-climate-model EMAC via the submodel PSC, Geosci. Model Dev., 4, 169–182, https://doi.org/10.5194/gmd-4-169-2011, 2011.

Knowland, K. E., Keller, C. A., Wales, P. A., Wargan, K., Coy, L., Johnson, M. S., Liu, J., Lucchesi, R. A., Eastham, S. D., Fleming, E., Liang, Q., Leblanc, T., Livesey, N. J., Walker, K. A., Ott, L. E., Pawson, S.: NASA GEOS Composition Forecast Modeling System GEOS-CF v1.0: Stratospheric Composition, J. Adv. Model. Earth Sy., 14, e2021MS002852, https://doi.org/10.1029/2021MS002852, 2022.

Kravitz, B., Robock, A., Boucher, O., Schmidt, H., Taylor, K. E., Stenchikov, G., and Schulz, M.: The geoengineering model intercomparison project (GeoMIP), Atmos. Sci. Lett., 12, 162–167, 2011.

Kulmala, M., Vehkamäki, H., Petäjä, T., Dal Maso, M., Lauri, A., Kerminen, V. M., Birmili, W., and McMurry, P. H.: Formation and growth rates of ultrafine atmospheric particles: a review of observations, J. Aerosol Sci., 35, 143–176, https://doi.org/10.1016/j.jaerosci.2003.10.003, 2004.

Kupc, A., Williamson, C., Wagner, N. L., Richardson, M., and Brock, C. A.: Modification, calibration, and performance of the Ultra-High Sensitivity Aerosol Spectrometer for particle size distribution and volatility measurements during the Atmospheric Tomography Mission (ATom) airborne campaign, Atmos. Meas. Tech., 11, 369–383, https://doi.org/10.5194/amt-11-369-2018, 2018.

Kupc, A., Williamson, C. J., Hodshire, A. L., Kazil, J., Ray, E., Bui, T. P., Dollner, M., Froyd, K. D., McKain, K., Rollins, A., Schill, G. P., Thames, A., Weinzierl, B. B., Pierce, J. R., and Brock, C. A.: The potential role of organics in new particle formation and initial growth in the remote tropical upper troposphere, Atmos. Chem. Phys., 20, 15037–15060, https://doi.org/10.5194/acp-20-15037-2020, 2020.

Kürten, A., Bianchi, F., Almeida, J., Kupiainen-Määttä, O., Dunne, E. M., Duplissy, J., Williamson, C., Barmet, P., Breitenlechner, M., Dommen, J., Donahue, N. M., Flagan, R. C., Franchin, A., Gordon, H., Hakala, J., Hansel, A., Heinritzi, M., Ickes, L., Jokinen, T., Kangasluoma, J., Kim, J., Kirkby, J., Kupc, A., Lehtipalo, K., Leiminger, M., Makhmutov, V., Onnela, A., Ortega, I. K., Petäjä, T., Praplan, A. P., Riccobono, F., Rissanen, M. P., Rondo, L., Schnitzhofer, R., Schobesberger, S., Smith, J. N., Steiner, G., Stozhkov, Y., Tomé, A., Tröstl, J., Tsagkogeorgas, G., Wagner, P. E., Wimmer, D., Ye, P., Baltensperger, U., Carslaw, K., Kulmala, M., and Curtius, J.: Experimental particle formation rates spanning tropospheric sulfuric acid and ammonia abundances, ion production rates, and temperatures, J. Geophys. Res.-Atmos., 121, 12377–12400, https://doi.org/10.1002/2015JD023908, 2016.

Laakso, A., Niemeier, U., Visioni, D., Tilmes, S., and Kokkola, H.: Dependency of the impacts of geoengineering on the stratospheric sulfur injection strategy – Part 1: Intercomparison of modal and sectional aerosol modules, Atmos. Chem. Phys., 22, 93–118, https://doi.org/10.5194/acp-22-93-2022, 2022.

Laakso, L., Gagné, S., Petäjä, T., Hirsikko, A., Aalto, P. P., Kulmala, M., and Kerminen, V.-M.: Detecting charging state of ultra-fine particles: instrumental development and ambient measurements, Atmos. Chem. Phys., 7, 1333–1345, https://doi.org/10.5194/acp-7-1333-2007, 2007.

Lee, S. H., Gordon, H., Yu, H., Lehtipalo, K., Haley, R., Li, Y., and Zhang, R.: New particle formation in the atmosphere: From molecular clusters to global climate, J. Geophys. Res.-Atmos., 124, 7098–7146, 2019.

Lee, S. H., Reeves, J. M., Wilson, J. C., Hunton, D. E., Viggiano, A. A., Miller, T. M., Ballenthin, J. O., and Lait, L. R.: Particle formation by ion nucleation in the upper troposphere and lower stratosphere, Science, 301, 1886–1889, https://doi.org/10.1126/science.1087236, 2003.

Li, M., Zhang, Q., Kurokawa, J.-I., Woo, J.-H., He, K., Lu, Z., Ohara, T., Song, Y., Streets, D. G., Carmichael, G. R., Cheng, Y., Hong, C., Huo, H., Jiang, X., Kang, S., Liu, F., Su, H., and Zheng, B.: MIX: a mosaic Asian anthropogenic emission inventory under the international collaboration framework of the MICS-Asia and HTAP, Atmos. Chem. Phys., 17, 935–963, https://doi.org/10.5194/acp-17-935-2017, 2017.

Lockley, A., MacMartin, D., and Hunt, H.: An update on engineering issues concerning stratospheric aerosol injection for geoengineering, Environmental Research Communications, 2, 082001, https://doi.org/10.1088/2515-7620/aba944, 2020.

Lovejoy, E. R., Curtius, J., and Froyd, K. D.: Atmospheric ion-induced nucleation of sulfuric acid and water, J. Geophys. Res., 109, D08204, https://doi.org/10.1029/2003JD004460, 2004.

Luo, G., Yu, F., and Moch, J. M.: Further improvement of wet process treatments in GEOS-Chem v12.6.0: impact on global distributions of aerosols and aerosol precursors, Geosci. Model Dev., 13, 2879–2903, https://doi.org/10.5194/gmd-13-2879-2020, 2020.

Martin, R. V., Jacob, D. J., Chance, K., Kurosu, T. P., Palmer, P. I., and Evans, M. J.: Global inventory of nitrogen oxide emissions constrained by space-based observations of NO_2 columns, J. Geophys. Res., 108, 4537, https://doi.org/10.1029/2003JD003453, 2003.

Mills, M. J., Richter, J. H., Tilmes, S., Kravitz, B., MacMartin, D. G., Glanville, A. A., Tribbia, J. J., Lamarque, J.-F., Vitt, F., Schmidt, A., and Gettelman, A.: Radiative and chemical response to interactive stratospheric sulfate aerosols in fully coupled CESM1 (WACCM), J. Geophys. Res., 122, 13061–13078, https://doi.org/10.1002/2017JD027006, 2017.

Murphy, D. M., Froyd, K. D., Schwarz, J. P., and Wilson, J. C.: Observations of the chemical composition of stratospheric aerosol particles, Q. J. Roy. Meteor. Soc., 140, 1269–1278. https://doi.org/10.1002/qj.2213, 2014.

Murphy, D. M., Froyd, K. D., Bourgeois, I., Brock, C. A., Kupc, A., Peischl, J., Schill, G. P., Thompson, C. R., Williamson, C. J., and Yu, P.: Radiative and chemical implications of the size and composition of aerosol particles in the existing or modified global stratosphere, Atmos. Chem. Phys., 21, 8915–8932, https://doi.org/10.5194/acp-21-8915-2021, 2021.

Murray, L. T., Jacob, D. J., Logan, J. A., Hudman, R. C., and Koshak, W. J.: Optimized regional and interannual variability of lightning in a global chemical transport model constrained by LIS/OTD satellite data, J. Geophys. Res., 117, D20307, https://doi.org/10.1029/2012JD017934, 2012.

Nadykto, A. B. and Yu, F.: Simple correction to the classical theory of homogeneous nucleation, J. Chem. Phys., 122, 104511, https://doi.org/10.1063/1.1861454, 2005.

NASEM: Reflecting Sunlight: Recommendations for Solar Geoengineering Research and Research Governance, The National Academies Press, Washington, DC, https://doi.org/10.17226/25762, 2021.

Pye, H. O. T. and Seinfeld, J. H.: A global perspective on aerosol from low-volatility organic compounds, Atmos. Chem. Phys., 10, 4377–4401, https://doi.org/10.5194/acp-10-4377-2010, 2010.

Richter, J. H., Visioni, D., MacMartin, D. G., Bailey, D. A., Rosenbloom, N., Dobbins, B., Lee, W. R., Tye, M., and Lamarque, J.-F.: Assessing Responses and Impacts of Solar climate intervention on the Earth system with stratospheric aerosol injection (ARISE-SAI): protocol and initial results from the first simulations, Geosci. Model Dev., 15, 8221–8243, https://doi.org/10.5194/gmd-15-8221-2022, 2022.

Rotman, D. A., Tannahill, J. R., Kinnison, D. E., Connell, P. S., Bergmann, D., Proctor, D., Rodriguez, J. M., Lin, S. J., Rood, R. B., Prather, M. J., Rasch, P. J., Considine, D. B., Ramaroson, R., and Kawa, S. R.: Global Modeling Initiative assessment model: Model description, integration, and testing of the transport shell, J. Geophys. Res.-Atmos., 106, 1669–1691, 2001.

Shepherd, J. G.: Geoengineering the climate: science, governance and uncertainty, Royal Society, ISBN: 9780854037735, 2009.

Shi, Q., Jayne, J. T., Kolb, C. E., Worsnop, D. R., and Davidovits, P.: Kinetic model for reaction of $ClONO_2$ with H_2O and HCl and HOCl with HCl in sulfuric acid solutions, J. Geophys. Res.-Atmos., 106, 24259–24274, 2001.

Stettler, M. E. J., Eastham, S., and Barrett, S. R. H.: Air quality and public health impacts of UK airports. Part I: Emissions, Atmos. Environ., 45, 5415–5424, 2011, 2011.

Stier, P., Feichter, J., Kinne, S., Kloster, S., Vignati, E., Wilson, J., Ganzeveld, L., Tegen, I., Werner, M., Balkanski, Y., Schulz, M., Boucher, O., Minikin, A., and Petzold, A.: The aerosol-climate model ECHAM5-HAM, Atmos. Chem. Phys., 5, 1125–1156, https://doi.org/10.5194/acp-5-1125-2005, 2005.

Sun, H., Eastham, S., and Keith, D.: Developing a Plume-in-Grid model for plume evolution in the stratosphere, J. Adv. Model. Earth Sy., 14, e2021MS002816, https://doi.org/10.1029/2021MS002816, 2022.

Svensmark, J., Shaviv, N. J., Enghoff, M. B., and Svensmark, H.: The ION-CAGE code: A numerical model for the growth of charged and neutral aerosols, Earth and Space Science, 7, e2020EA001142, https://doi.org/10.1029/2020EA001142, 2020.

The International GEOS-Chem User Community: geoschem/geos-chem: GEOS-Chem 12.6.0, Version 12.6.0, Zenodo [code], https://doi.org/10.5281/zenodo.3507501, 2019.

Thompson, C. R., Wofsy, S. C., Prather, M. J., Newman, P. A., Hanisco, T. F., Ryerson, T. B., Fahey, D. W., Apel, E. C., Brock, C. A., Brune, W. H., Froyd, K., Katich, J. M., Nicely, J. M., Peischl, J., Ray, E., Veres, P. R., Wang, S., Allen, H. M., Asher, E., Bian, H., Blake, D., Bourgeois, I., Budney, J., Bui, T. P., Butler, A., Campuzano-Jost, P., Chang, C., Chin, M., Commane, R., Correa, G., Crounse, J. D., Daube, B., Dibb, J. E., DiGangi, J. P., Diskin, G. S., Dollner, M., Elkins, J. W., Fiore, A. M., Flynn, C. M., Guo, H., Hall, S. R., Hannun, R. A., Hills, A., Hintsa, E. J., Hodzic, A., Hornbrook, R. S., Huey, L. G., Jimenez, J. L., Keeling, R. F., Kim, M. J., Kupc, A., Lacey, F., Lait, L. R., Lamarque, J., Liu, J., McKain, K., Meinardi, S., Miller, D. O., Montzka, S. A., Moore, F. L., Morgan, E. J., Murphy, D. M., Murray, L. T., Nault, B. A., Neuman, J. A., Nguyen, L., Gonzalez, Y., Rollins, A., Rosenlof, K., Sargent, M., Schill, G., Schwarz, J. P., Clair, J. M. S., Steenrod, S. D., Stephens, B. B., Strahan, S. E., Strode, S. A., Sweeney, C., Thames, A. B., Ullmann, K., Wagner, N., Weber, R., Weinzierl, B., Wennberg, P. O., Williamson, C. J., Wolfe, G. M., and Zeng, L.: The NASA Atmospheric Tomography (ATom) Mission: Imaging the Chemistry of the Global Atmosphere, B. Am. Meteorol. Soc., 103, E761–E90, 2022.

Tilmes, S., Mills, M. J., Niemeier, U., Schmidt, H., Robock, A., Kravitz, B., Lamarque, J.-F., Pitari, G., and English, J. M.: A new Geoengineering Model Intercomparison Project (GeoMIP) experiment designed for climate and chemistry models, Geosci. Model Dev., 8, 43–49, https://doi.org/10.5194/gmd-8-43-2015, 2015.

Turco, R. P., Whitten, R. C., and Toon, O. B.: Stratospheric aerosols: Observation and theory, Rev. Geophys., 20, 233–279, https://doi.org/10.1029/RG020i002p00233, 1982.

van der Werf, G. R., Randerson, J. T., Giglio, L., van Leeuwen, T. T., Chen, Y., Rogers, B. M., Mu, M., van Marle, M. J. E., Morton, D. C., Collatz, G. J., Yokelson, R. J., and Kasibhatla, P. S.: Global fire emissions estimates during 1997–2016, Earth Syst. Sci. Data, 9, 697–720, https://doi.org/10.5194/essd-9-697-2017, 2017.

van Donkelaar, A., Martin, R. V., Leaitch, W. R., Macdonald, A. M., Walker, T. W., Streets, D. G., Zhang, Q., Dunlea, E. J., Jimenez, J. L., Dibb, J. E., Huey, L. G., Weber, R., and Andreae, M. O.: Analysis of aircraft and satellite measurements from the Intercontinental Chemical Transport Experiment (INTEX-B) to quantify long-range transport of East Asian sulfur to Canada, Atmos. Chem. Phys., 8, 2999–3014, https://doi.org/10.5194/acp-8-2999-2008, 2008.

Vehkamäki, H., Kulmala, M., Napari, I., Lehtinen, K. E., Timmreck, C., Noppel, M., and Laaksonen, A.:. An improved parameterization for sulfuric acid–water nucleation rates for tropospheric and stratospheric conditions, J. Geophys. Res., 107, 4622, https://doi.org/10.1029/2002JD002184, 2002.

Weisenstein, D. K., Visioni, D., Franke, H., Niemeier, U., Vattioni, S., Chiodo, G., Peter, T., and Keith, D. W.: An interactive stratospheric aerosol model intercomparison of solar geoengineering by stratospheric injection of SO_2 or accumulation-mode sulfuric acid aerosols, Atmos. Chem. Phys., 22, 2955–2973, https://doi.org/10.5194/acp-22-2955-2022, 2022.

Williamson, C., Kupc, A., Wilson, J., Gesler, D. W., Reeves, J. M., Erdesz, F., McLaughlin, R., and Brock, C. A.: Fast time response measurements of particle size distributions in the 3–60 nm size range with the nucleation mode aerosol size spectrometer, Atmos. Meas. Tech., 11, 3491–3509, https://doi.org/10.5194/amt-11-3491-2018, 2018.

Williamson, C. J., Kupc, A., Axisa, D., Bilsback, K. R., Bui, T., Campuzano-Jost, P., Dollner, M., Froyd, K. D., Hodshire, A. L., Jimenez, J. L., Kodros, J. K., Luo, G., Murphy, D. M., Nault, B. A., Ray, E. A., Weinzierl, B., Wilson, J. C., Yu, F. Q., Yu, P. F., Pierce, J. R., and Brock, C. A.: A large source of cloud condensation nuclei from new particle formation in the tropics, Nature, 574, 399–403, https://doi.org/10.1038/s41586-019-1638-9, 2019.

Williamson, C. J., Kupc, A., Rollins, A., Kazil, J., Froyd, K. D., Ray, E. A., Murphy, D. M., Schill, G. P., Peischl, J., Thompson, C., Bourgeois, I., Ryerson, T. B., Diskin, G. S., DiGangi, J. P., Blake, D. R., Bui, T. P. V., Dollner, M., Weinzierl, B., and Brock, C. A.: Large hemispheric difference in nucleation mode aerosol concentrations in the lowermost stratosphere at mid- and high latitudes, Atmos. Chem. Phys., 21, 9065–9088, https://doi.org/10.5194/acp-21-9065-2021, 2021.

Wofsy, S. C., Afshar, S., Allen, H. M., Apel, E. C., Asher, E. C., Barletta, B., Bent, J., Bian, H., Biggs, B. C., Blake, D. R., Blake, N., Bourgeois, I., Brock, C. A., Brune, W. H., Budney, J. W., Bui, T. P., Butler, A., Campuzano-Jost, P., Chang, C. S., Chin, M., Commane, R., Correa, G., Crounse, J. D., Cullis, P. D., Daube, B. C., Day, D. A., Dean,Day, J. M., Dibb, J. E., DiGangi, J. P., Diskin, G. S., Dollner, M., Elkins, J. W., Erdesz, F., Fiore, A. M., Flynn, C. M., Froyd, K. D., Gesler, D. W., Hall, S. R., Hanisco, T. F., Hannun, R. A., Hills, A. J., Hintsa, E. J., Hoffman, A., Hornbrook, R. S., Huey, L.G., Hughes, S., Jimenez, J. L., Johnson, B. J., Katich, J. M., Keeling, R. F., Kim, M. J., Kupc, A., Lait, L. R., McKain, K., Mclaughlin, R. J., Meinardi, S., Miller, D. O., Montzka, S. A., Moore, F. L., Morgan, E. J., Murphy, D. M., Murray, L. T., Nault, B. A., Neuman, J. A., Newman, P. A., Nicely, J. M., Pan, X., Paplawsky, W., Peischl, J., Prather, M. J., Price, D. J., Ray, E. A., Reeves, J. M., Richardson, M., Rollins, A. W., Rosenlof, K. H., Ryerson, T. B., Scheuer, E., Schill, G. P., Schroder, J. C., Schwarz, J. P., St.Clair, J. M., Steenrod, S. D., Stephens, B. B., Strode, S. A., Sweeney, C., Tanner, D., Teng, A. P., Thames, A. B., Thompson, C. R., Ullmann, K., Veres, P. R., Wagner, N. L., Watt, A., Weber, R., Weinzierl, B. B., Wennberg, P. O., Williamson, C. J., Wilson, J. C., Wolfe, G. M., Woods, C. T., Zeng, L. H., and Vieznor, N.: ATom: Merged Atmospheric Chemistry, Trace Gases, and Aerosols, Version 2, ORNL DAAC [data set], Oak Ridge, Tennessee, USA, https://daac.ornl.gov/ATOM/campaign/ (last access: 30 June 2022), 2021.

Yu, F.: Particle number concentrations and size distributions in the stratosphere: Implications of nucleation mechanisms and particle microphysics, Zenodo [data set], https://doi.org/10.5281/zenodo.6909944, 2022.

Yu, F. and Luo, G.: Simulation of particle size distribution with a global aerosol model: contribution of nucleation to aerosol and CCN number concentrations, Atmos. Chem. Phys., 9, 7691–7710, https://doi.org/10.5194/acp-9-7691-2009, 2009.

Yu, F. and Turco, R. P.: Ultrafine aerosol formation via ion-mediated nucleation, Geophys. Res. Lett., 27, 883–886, https://doi.org/10.1029/1999GL011151, 2000.

Yu, F. and Turco, R.: Case studies of particle formation events observed in boreal forests: implications for nucleation mechanisms, Atmos. Chem. Phys., 8, 6085–6102, https://doi.org/10.5194/acp-8-6085-2008, 2008.

Yu, F., Nadykto, A. B., Herb, J., Luo, G., Nazarenko, K. M., and Uvarova, L. A.: H_2SO_4–H_2O–NH_3 ternary ion-mediated nucleation (TIMN): kinetic-based model and comparison with CLOUD measurements, Atmos. Chem. Phys., 18, 17451–17474, https://doi.org/10.5194/acp-18-17451-2018, 2018.

Yu, F., Nadykto, A. B., Luo, G., and Herb, J.: H_2SO_4–H_2O binary and H_2SO_4–H_2O–NH_3 ternary homogeneous and ion-mediated nucleation: lookup tables version 1.0 for 3-D modeling application, Geosci. Model Dev., 13, 2663–2670, https://doi.org/10.5194/gmd-13-2663-2020, 2020.

Zhang, R., Khalizov, A., Wang, L., Hu, M., and Xu, W.: Nucleation and growth of nanoparticles in the atmosphere, Chem. Rev., 112, 1957–2011, 2012.